ACS Sustainable Chemistry & Engineering

Research Article

pubs.acs.org/journal/ascecg

Biomimetic Controlling of $CaCO_3$ and $BaCO_3$ Superstructures by Zwitterionic Polymer

Shengjie Xu, Zhangxin Ye, and Peiyi Wu*

State Key Laboratory of Molecular Engineering of Polymers, Collaborative Innovation Center of Polymers and Polymer Composite Materials, Department of Macromolecular Science and Laboratory for Advanced Materials, Fudan University, Shanghai 200433, China

Supporting Information

ABSTRACT: In this work, uniform calcium carbonate ($CaCO_3$) and barium carbonate ($BaCO_3$) crystals were synthesized under the control of poly(2-methacryloyloxyethylphosphorylcholine) (PMPC) via a simple gas−liquid diffusion reaction. Spherical $CaCO_3$ particles with six smooth facets symmetrically distributed on the surface were prepared and systemically characterized by means of TEM, SEM, XRD, Raman, TGA, and FTIR. Time-resolved experiments showed the spherical calcite crystals were transformed from amorphous calcium carbonate (ACC) in the early stage and underwent a dissolution−recrystallization process in the later stage. For $BaCO_3$, dumbbell-shaped crystals that were formed by the dendritic aggregation of rod-like subunits with six sides were generated. Both the morphologies of $CaCO_3$ and $BaCO_3$ crystals could be effectively tuned by changing the crystallization time and concentration of PMPC. Finally, a possible crystallization mechanism for the formation of $CaCO_3$ and $BaCO_3$ particles under the control of PMPC was proposed based on the experiments.

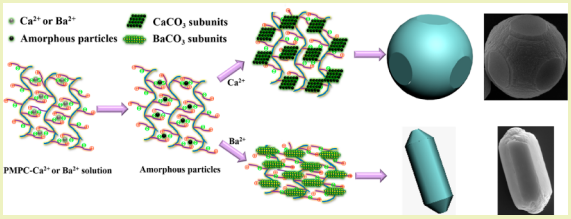

KEYWORDS: *Zwitterionic, Poly(2-methacryloyloxyethylphosphorylcholine), Time-resolved experiments, Spherical calcite with six planes, Dendritic $BaCO_3$*

INTRODUCTION

In nature, biominerals are biogenic materials made by the orderly stacking of inorganics. The size, shape, and crystallographic orientation of biominerals can be accurately regulated by polysaccharides or proteins in living organisms.[1−4] Among these biominerals, $CaCO_3$ is most researched by scientists due to it being the basis and crucial constituent for nacre, which is one of the most impressive materials formed in the natural environment with a highly regular brick-and-mortar arrangement structure and excellent mechanical properties.[3,5] Moreover, $CaCO_3$ has already been widely used in many industrial areas for hundreds of years, like papermaking, plastics, paints, cosmetics, rubber industry, etc.; hence, how to control the size, morphology, and mechanical properties of $CaCO_3$ particles has drawn great attention.[4,6,7]

To investigate the mineralization mechanism and artificially synthesize $CaCO_3$ with regular structure and excellent mechanical property, plenty of biomimetic strategies have been employed. The most crucial factor for these strategies is the use of water-soluble modifiers; a significant amount of work has demonstrated that water-soluble modifiers can stabilize the amorphous calcium carbonate (ACC), accelerate the growth, and regulate the morphology and polymorphs of $CaCO_3$ crystals.[8−13] Up to now, water-soluble modifiers provided one of the most versatile methods for controlling the crystallization process of $CaCO_3$ crystals and other minerals.[9,14−17] Protein is regarded as the most suitable modifier to regulate the morphology, polymorphs, and texture of $CaCO_3$ crystals because the specific function of the biominerals are always formed under the control of protein in organisms; however, the limitation of water-soluble protein in nature hinders the widespread use of it.[18−20] To overcome this problem, much attention has been paid on artificially synthesizing water-soluble proteins or polypeptides to replace the role of natural protein. But the high cost, harsh reaction conditions, and low conversion yield of condensation polymerization of amino acids hamper the wide use of these methods.[21−23] To date, the most utilized modifiers are polyelectrolytes, which are generated by additional polymerization and contain positive or negative charges on each side chain, such as poly(acrylic acid) (PAA), poly(sodium 4-styrenesulfonate) (PSS), poly(allylamine hydrochloride) (PAH), sodium salts of carboxymethyl cellulose (NaCMC), etc.[10,13,17,24,25] Various morphologies of $CaCO_3$ can be generated under the control of these polyelectrolytes. However, as far as we know, most of these polyelectrolytes have only one kind of charge; compared to protein, they are not very suitable to use to investigate the mineralization mechanism under the control of protein in organisms and biomimetically synthesize biominerals.

Phosphorylcholine is a crucial component of phospholipids that act as a key role in cell membranes.[26,27] 2-Methacryloyloxyethylphosphorylcholine (MPC) is the most researched

Received: May 3, 2015
Revised: June 8, 2015
Published: June 18, 2015

DOI: 10.1021/acssuschemeng.5b00387
ACS Sustainable Chem. Eng. 2015, 3, 1810−1818

phosphorylcholine during the past few decades. It is an excellent monomer from the viewpoint of polymerization ability, and the polymers of it are regarded as one of the most suitable phospholipids moieties for the study of the stabilization of phospholipid assemblies.[28,29] As previous works reported, poly(2-methacryloyloxyethylphosphorylcholine) (PMPC) shows extremely high biocompatibility and antithrombogenicity, which has already been applied for implantable medical devices and drugs delivery.[29−31] Importantly, MPC has both positive and negative charges, which is similar to amino acids, thereby, to some extent, the property of zwitterionic PMPC is close to proteins or polypeptides. Moreover, the excellent water solubility and dispersibility, strong intermolecular association through electrostatic interaction, and high affinity for metal salts determine that PMPC can be an ideal and promising substitute for proteins or polypeptides to biomimetically synthesize $CaCO_3$ crystals and investigate the mineralization mechanism of $CaCO_3$ in organisms.[2,27,32,33]

Herein, we proposed a biomimetic synthetic method to fabricate $CaCO_3$ and $BaCO_3$ crystals with delicate morphology through a simple gas−liquid diffusion reaction of carbon dioxide (CO_2) in the presence of a zwitterionic polymer, PMPC, as the nucleation and growth modifier. Uniform spherical $CaCO_3$ crystals with six smooth facets symmetrically distributed on surface and dumbbell-shaped $BaCO_3$ crystals that were formed by the dendritic aggregation of rod-like subunits with six sides were generated under the control of PMPC. Besides, the morphology of $CaCO_3$ and $BaCO_3$ crystals could be efficiently tuned by the mineralization time and the concentration of PMPC. Because PMPC both contains positive and negative charges, which is similar to protein, our work might provide a new view to the investigation of the mechanism of biomimetic mineralization under the control of protein.

EXPERIMENTAL SECTION

Materials. Calcium chloride ($CaCl_2$), barium chloride ($BaCl_2$), ammonium carbonate ($(NH_4)_2CO_3$), and potassium peroxydisulfate (KPS) were purchased from Sinopharm Chemical Reagent Co., Ltd. 2-Methacryloyloxyethyl phosphorylcholine (MPC) was purchased from Joy-Nature Technology Institute. All reagents were of analytical grade and used without further purification.

Synthesis of PMPC. PMPC was synthesized by typical radical polymerization. Briefly, 0.5905 g of MPC was dissolved in 20 mL of deionized water, followed by adding 0.0027 g of KPS, and then the mixture was kept at 60 °C in N_2 atmosphere for 4 h in oil−water bath. Afterward, the mixture was dialyzed in deionized water by using a Slide-a-Lyzer dialysis cassette (molecular weight cutoff, MWCO, 14000) for at least 7 days to remove residual MPC. Finally, the product was freeze-dried for characterization.

Preparation of $CaCO_3$ and $BaCO_3$ Crystals under the Control of PMPC. All glassware (small pieces of glass slides and glass bottles) were subjected to ethanol and sonicated for 15 min, rinsed with deionized water, followed by soaking in HNO_3−H_2O_2−H_2O (1:1:1) solution for 24 h, further cleaned with deionized water and acetone, and finally dried in oven at 60 °C.

The mineralization process was carried out with a gas-diffusion method, which had been reported in our previous work.[34] Typically, 10 mL of 0.01 M $CaCl_2$ (or $BaCl_2$) solution was added into a 10 mL beaker, followed by 0.05 g of PMPC. Two pieces of clean glass slides were carefully put at the bottom of the beaker. Then, the beaker was covered with parafilm, which was pierced with three needle holes; afterward, the beaker was placed into a closed desiccator with a bottle of $(NH_4)_2CO_3$ powder at the bottom. After different mineralization times, the beaker was taken out of desiccator, the glass slides were carefully taken out, and the product was rinsed with ethanol or deionized water and dried at ambient conditions for further characterization.

Characterization. The scanning electron microscope (SEM) images were taken with Zeiss Ultra 55 microscope and Hitachi-S-4800 FE-SEM with gold coating. Transmission electron microscope (TEM) observations were carried out on a JEOL JEM2011 at 200 kV equipped with selective area electron diffraction (SAED). Raman spectra were recorded on a Renishaw inVia Reflex Raman spectrometer equipped with 632.8 nm helium/neon laser and CCD detector. Thermogravimetric analysis (TGA) was performed at a heating rate of 20 K/min on PerkinElmer Pyris-1 TGA in a nitrogen atmosphere at a flow rate of 40 cm^3/min. Fourier transform infrared (FTIR) spectra were taken with a Nicolet Nexus 470 spectrometer. ^1H nuclear magnetic resonance (^1H NMR) spectra were recorded on a Bruker AVANCE 400-MHz instrument by using D_2O as solvent and TMS as an internal standard.

RESULTS AND DISCUSSION

Synthesis and Characterizations of PMPC. PMPC was synthesized by a simple radical polymerization employing KPS as initiator.[27] Figure 1 shows the ^1H NMR spectra of MPC

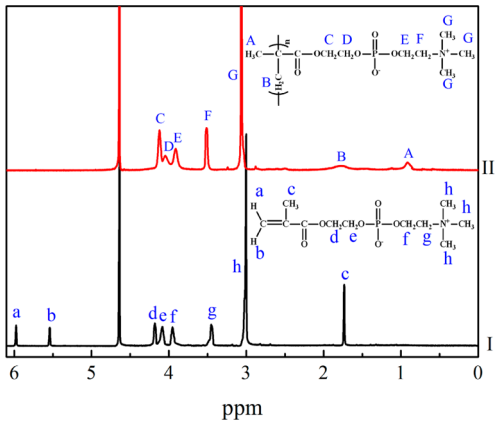

Figure 1. ^1H NMR spectra of MPC (I) and PMPC (II).

monomer (I) and as-prepared PMPC (II) with the relevant signals labeled. The resonance peaks at 3.5, 3.9, 4.1, and 4.2 ppm are assigned to phosphorylcholine moieties, and the peaks at 5.6 and 6.0 ppm are attributed to unsaturated double bond moieties of MPC units. After polymerization, these peaks disappear, and instead, a broad band is observed at 1.8 ppm, which is assigned to the methylene groups on the main chain, as well as the characteristic peak of the methyl groups shift from 1.7 to 1.0 ppm.[26,31] FTIR spectra were also utilized to characterize the structure of MPC and PMPC. As shown in Figure 2, the peak at 1721 cm^{-1} refers to C═O groups, 1242 and 1088 cm^{-1} are attributed to $-POCH_2$ groups, and 966 cm^{-1} is associated with $-N^+(CH_3)_3$ groups. Moreover, the peaks at 1633 and 1303 cm^{-1}, which are assigned to ν(C═C) and ν(═C−H) of MPC, disappear after polymerization, indicating PMPC is successfully synthesized.[26,35,36] The improvement of pyrolysis temperature after polymerization also reveals that MPC is polymerized to PMPC (Figure S1, Supporting Information).

Effect of PMPC Concentration on Morphology of $CaCO_3$ Crystals. To investigate the effect of PMPC concentration on the morphology of $CaCO_3$ crystals, a series of PMPC aqueous solutions from 0.1 to 15 g/L were used. The SEM images of these crystals are shown in Figure 3. Typical rhombohedron particles with a size of 35 μm are generated

DOI: 10.1021/acssuschemeng.5b00387
ACS Sustainable Chem. Eng. 2015, 3, 1810−1818

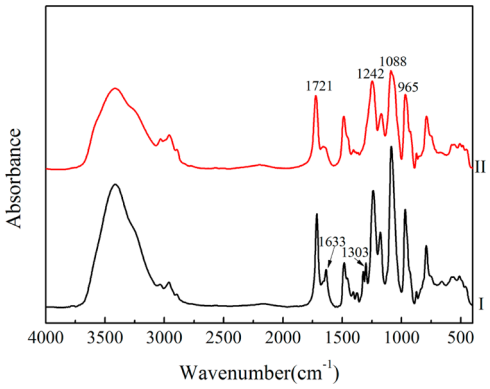

Figure 2. FTIR spectra of MPC (I) and PMPC (II).

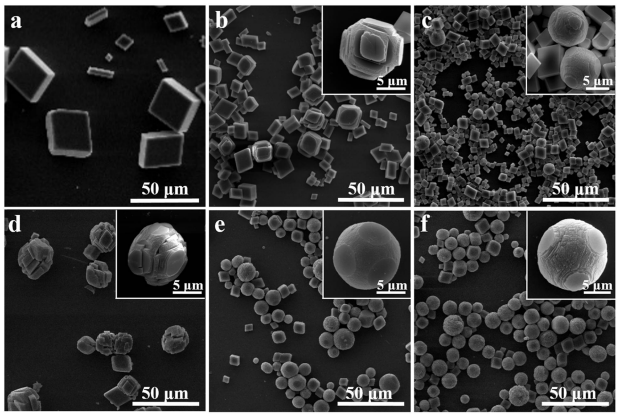

Figure 3. SEM images of $CaCO_3$ particles generated in different PMPC solution at 25 °C: (a) 0.1, (b) 1, (c) 3, (d) 5, (e) 10, and (f) 15 g/L.

when the concentration of PMPC is very low (0.1 g/L), which is very similar to the samples prepared without any modifier.[4] When the concentration is 1 g/L, most of crystals are still rhombohedron. However, some of them begin to evolve complex morphologies with terraced structures on the surface, and the edges and corners become fuzzy. With increasing PMPC concentration to 3 and 5 g/L, the edges and corners of particles become more fuzzy and their surfaces become smoother, together with the particles tending to form spheres. Moreover, their sizes decreases to 10 μm, revealing that PMPC begins to regulate the nucleation and growth of $CaCO_3$ crystals. When the concentration of PMPC is increased to 10 g/L, the particles form spheres with six smooth facets symmetrically distributed on their surfaces, which is close to the morphology of $CaCO_3$ prepared in the presence of poly(4-styrenesulfonate-*co*-maleic acid) (PSS-*co*-MA) by Colfen et al.[9] Noticeably, the six-sided structure is similar to calcite's equilibrium shape, which is rhombohedron in some ways. The particles that are generated with 15 g/L PMPC hardly change compared with particles fabricated in 10 g/L PMPC solution, in spite of the proportion of the spheres improving. These results indicate that PMPC can effectively regulate $CaCO_3$ particles to spheres with six smooth facets symmetrically distributed on the surface, and the critical concentration of PMPC for this morphology is about 10 g/L. To confirm our speculation, we also prepared $CaCO_3$ crystals in two different PMPC solutions whose concentrations were close to 10 g/L (7.5 and 12.5 g/L) (Figure S2, Supporting Information). The results show that the $CaCO_3$ particles prepared in 7.5 g/L PMPC solution are still irregular, and uniform spherical $CaCO_3$ can be prepared in 12.5 g/L PMPC solution. This means that spherical $CaCO_3$ particles with six smooth facets symmetrically distributed on the surface can only be prepared when the concentration of PMPC is higher than 10 g/L.

X-ray powder diffraction (XRD) and Raman spectrometer were employed to systematically investigate the polymorphs of $CaCO_3$ crystals generated in different PMPC solutions. The XRD patterns show that all of the particles prepared with PMPC are calcite, and the main peak at 29.2° (d-spacing = 3.02 Å) is assigned to the (104) face of calcite (Figure 4a).[37] In the Raman spectra, the peaks at 1085 and 711 cm^{-1} are assigned to symmetric stretching (ν_1) and in-plane bending (ν_4) of calcite, and the two peaks located at 281 and 155 cm^{-1} are attributed to the lattice vibration of calcite, also indicating that all of the $CaCO_3$ crystals regulated by PMPC are calcite (Figure 4b).[38] As we know, the usual morphology of calcite is rhombohedron, due to the unit cell of calcite belong to the trigonal phase.[17] In the present work, the spherical calcite particles are probably formed by the orderly stack of rhombohedral subunits under the control of PMPC chains. The six-sided structure of these spheres is similar to a rhombohedron in some ways, partly confirming this speculation (Figure 3e). In order to demonstrate the regulatory effect of PMPC, the content of PMPC in the products were measured by TGA analyses (Figure 4c and Table S1, Supporting Information). In Figure 4c, two weight loss sections can be observed, the maximum weight one occurs from 600 to 800 °C, assigned to the thermal decomposition of $CaCO_3$ crystals.[39,40] The other one, which takes place from 280 to 500 °C, should be ascribed to the thermal pyrolysis of the PMPC skeleton (Figure S1, Supporting

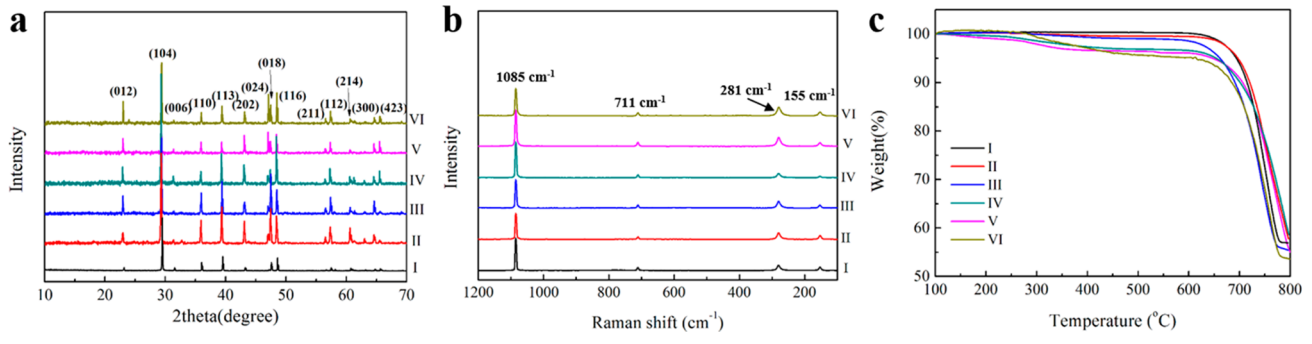

Figure 4. (a) XRD patterns, (b) Raman spectra, and (c) TGA curves of $CaCO_3$ particles generated in different PMPC solutions at 25 °C: (I) 0.1, (II) 1, (III) 3, (IV) 5, (V) 10, and (VI) 15 g/L.

DOI: 10.1021/acssuschemeng.5b00387
ACS Sustainable Chem. Eng. 2015, 3, 1810−1818

Information).[41] Interestingly, the specific content of PMPC in $CaCO_3$ and $BaCO_3$ crystals is enhanced with an increase in initially adding PMPC and a much higher initial concentration. This distinctly reveals that PMPC chains take part in and regulate the nucleation and growth of $CaCO_3$ particles during the crystallization process. This result is further confirmed by FTIR spectra. The peaks at 1721 and 1088 cm^{-1}, which are attributed to C═O groups and $-POCH_2$ groups of PMPC, can be observed in the FTIR spectrum of the as-prepared $CaCO_3$ particles, indicating that PMPC chains are still embedded in the $CaCO_3$ particles after crystallization (Figure S3, Supporting Information).[25,34,35]

Time-Resolved Experiments of $CaCO_3$ Crystallization Process. Time-resolved experiments were performed in a 15 g/L PMPC solution to investigate the crystallization process of $CaCO_3$ under the control of PMPC. Figure 5 shows the TEM images of $CaCO_3$ particles generated after different mineralization times. Noticeably, two kinds of particles are observed in the initial stage (0.5 h) (Figure 5a). For the low contrast particle, no crystal lattice can be found in the high resolution TEM (HRTEM) image, indicating the particle is amorphous calcium carbonate (ACC), which is certified by the dispersion ring on the SAED pattern (Figure 5b).[42,43] While for the other particle in Figure 5a, the clear and order lattice fringes in HRTEM reveal that the particle is well crystallized, and the *d*-spacing is 3.02 Å, corresponding to the (104) faces of calcite (Figure 5c).[37] The single-crystalline SAED pattern with sharp faculae also reveals that the crystal has high crystallographic orientation. The faculae are assigned to (104), (102), and (006) faces of calcite, suggesting ACC transforms to calcite gradually during the mineralization process.[19,24,44] When the reaction time is increased to 1.5 h, the particles become bigger, although the morphology is still irregular and blurry; the order lattice fringes and single-crystalline SAED pattern with sharp and bright faculae indicate almost all the particles are well crystallized (Figure 5d and e). With prolonging the mineralization time to 2 h, the crystals form a sphere with a rough texture (Figure 5f). Moreover, the HRTEM image and SAED pattern also show that these particles are calcite with high crystallographic orientation (Figure 5g). Remarkably, the crystals are probably composed of many distinct nanocrystalline domains because the orientation in Figure 5g is not the same; however, the lattice fringes are still very defined and well ordered, which are characteristic of a so-called "'mesocrystal"', that is, a mesocrystal is usually formed by the stacking of plenty of single crystals and scatters like a single crystal whose subunits are aligned crystallographically, which will easily turn into single crystals through the fusion process.[17,45−47]

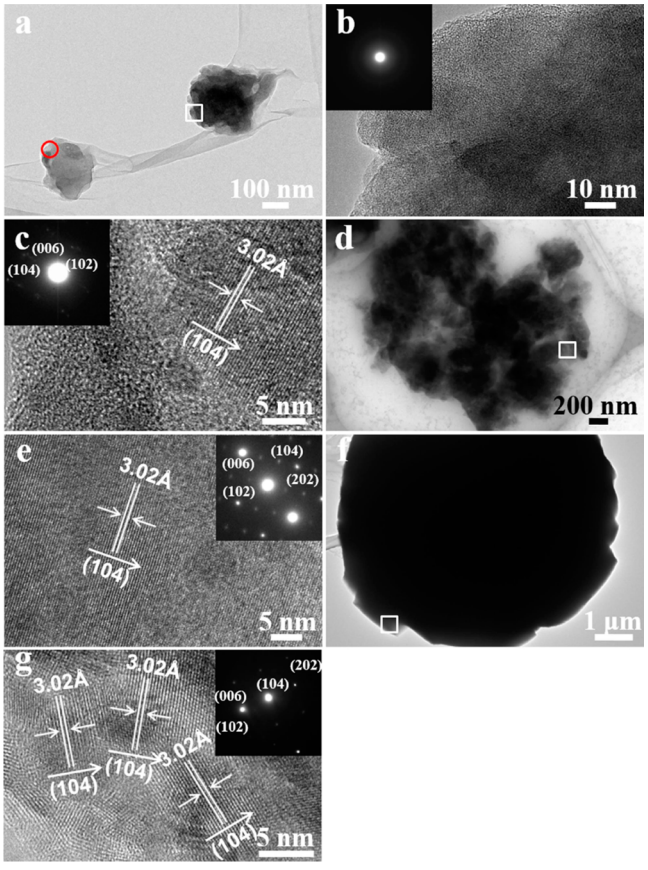

Figure 5. TEM images of $CaCO_3$ particles generated in 15 g/L PMPC solution after different mineralization times at 25 °C: (a, b, c) 0.5 h, (d, e) 1.5 h, and (f, g) 2 h. Panels (b) and (c) are the HRTEM images of the marked area of (a) with red color and white color, respectively. Panels (e) and (g) are the HRTEM images of the marked area of (d) and (f). The insets show the SAED patterns of each sample.

Because the particles are completely turned into spheres and the polymorphs of them are transformed to calcite after more than 2 h mineralization, SEM is more suitable to investigate the morphology and detailed surface structure of the crystals. Besides, the SEM images of products prepared in the early stage are also obtained to certify the results of TEM images (0.5, 1, 1.5, and 2 h), as shown in Figure 6a, b, c, and d. When the reaction time is shorter than 2 h, the particles are irregular and very small, which is well consistent with the results in the TEM images. Spherical crystals with rough and complex texture on the surface are first observed when the mineralization time is 2 h, and some initial facets are found on the particle surface (Figure 6d). Importantly, the enlarged image shows these spherical crystals are stacked by many subunits, which is in accord with the result in Figure 5g, that is, the crystal is a mesocrystal and formed by the stacking of single crystals (Figure S4a, Supporting Information). Moreover, The EDS pattern shows that these particles are composed of C, O, and

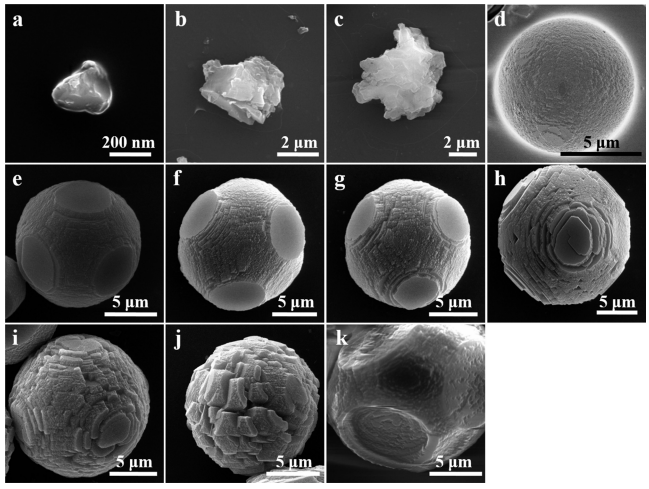

Figure 6. SEM images of $CaCO_3$ crystals prepared after different mineralization time in 15 g/L PMPC solution at 25 °C: (a) 0.5, (b) 1, (c) 1.5, (d) 2, (e) 3, (f) 4.5, (g) 6, (h) 9, (i) 12, (j) 18, and (k) 36 h.

DOI: 10.1021/acssuschemeng.5b00387
ACS Sustainable Chem. Eng. 2015, 3, 1810−1818

Ca elements, confirming all of them are $CaCO_3$ particles (Figure S5, Supporting Information). When the reaction time is increased to 3 h, uniform spheres with six smooth facets symmetrically distributed on surface begin to appear, and the sizes of them increase to 10 μm (Figure 6e and Figure S4b, Supporting Information). As we know, the usual morphology of calcite is rhombohedron, which also has six smooth facets. Thereby, the six-faceted shape in the present work probably is the intrinsic morphology of rhombohedron crystal, and these facets should be the most favorite and low-energy crystal facet of calcite. The integral spherical morphology of these particles should result from control of the PMPC modifier; in other words, PMPC chains take part in the growth of crystals and regulate the ordered stacking of rhombohedron subunits to form spheres. Besides, a sphere always is the most stable and favorite morphology based on the lowest energy principle. For the crystals prepared after 4.5 and 6 h reactions, the morphologies are almost the same with the crystals obtained after 3 h; however, the size slightly increases to 12 μm and the surface becomes rougher (Figure 6f, g and Figure S4c, d, Supporting Information). As the mineralization time is increased to 9 h, the surface of the particles becomes rough, as well as some defects appearing on the smooth facets (Figure 6h and Figure S4e, Supporting Information). These morphological changes might result from two factors. The first one is that the modifying polymer becomes consumed and the regulated effect is weakened over the reaction time course, thereby a new mode of growth (crystal faceting) begins once the concentration of polymer in the solution is dropped. Thus, further morphological change might result from the crystal's spontaneous overgrowth from the nanocrystalline seeds present at the mesocrystal surface. The second one is the dissolution of some crystals whose crystal lattices are partly defected by PMPC chains. This speculation is certified by the crystal prepared after 12 h mineralization because as shown the surface becomes more rugged and the area of facets on the surface are sharply decreased (Figure 6i and Figure S4f, Supporting Information), suggesting the fusion of defected crystals. However, the crystals become more spherical, which indicates the further growth of nanocrystals on the crystal surface. When the reaction time is 18 h, the corrosion is continually enhanced and the facets almost disappear. Noticeably, part of the crystals are sharply etched (sunken area), but some of them are slightly etched (embossment area) (Figure 6j and Figure S4g, Supporting Information). This might also result from the fusion of defected crystals that are intercalated with PMPC chains and the growth of new crystals on part of the surface. Generally, the crystals that have residual PMPC chains should be fused easily because the crystal lattices are partly defected by polymer chains. While for other crystals without PMPC chains, the crystals are perfect. The solvent is not easy to permeate into the crystals, so the fusion is not very evident. Moreover, the crystals would like to continue to grow in these regions. However, when the mineralization time is very long, the dissolution of defected crystals becomes much stronger, and the growth of new crystals is weakened because of a decrease in Ca^{2+} ions, which has already been demonstrated by previous reports.[37,48] Therefore, both defected and perfect crystals would be sharply etched in the later stage, which can be certified by the products generated after 36 h reaction (Figure 6k and Figure S4h, Supporting Information). The rugged surface disappears, and instead, the sunken and relatively smooth surface with some textured structure is formed because of the strong fusion for all parts of the crystal.

The Raman spectra of $CaCO_3$ crystals generated after 1.5 to 36 h are recorded (Figure S6, Supporting Information). The results show all of the crystals prepared with 15 g/L PMPC after different mineralization times are calcite, indicating that the most favorite and stable polymorph of the $CaCO_3$ crystal regulated by PMPC is calcite, and this polymorph is formed in the early stage and is not changed during the growth process. Moreover, the enhancement of characteristic peak intensity with an increase in reaction time also suggests the crystallinity of particles is increased during the growth process.

Regulatory Effect of PMPC on Morphology of $BaCO_3$ Crystals. In order to investigate the regulatory effect of PMPC on other metal carbonates, $BaCO_3$ crystals were selected as the representative and fabricated in different PMPC solutions. When PMPC concentration is very low (1 g/L), vimineous branches are fabricated after 3 h, which is similar to the intrinsic morphology of $BaCO_3$ crystals prepared in deionized water directly (Figure S7a, Supporting Information). With an increase in reaction time, their morphology does not change distinctly, although some of them are aggregated, suggesting that the concentrations of PMPC are not high enough to efficiently control the morphology of $BaCO_3$ (Figure S7b and c, Supporting Information). When the concentration of PMPC is 5 g/L, spindle-shaped particles are prepared, although the length of them is almost unchanged compared with the products in 1g/L PMPC solution and the width of them obviously increases (Figure S7d and e, Supporting Information). When the reaction time is prolonged to 18 h, several particles stack together to form dendritic structure (Figure S7f, Supporting Information). These results reveal that PMPC begins to influence and control the morphology of $BaCO_3$ particles at this concentration, which is well consistent with the result in $CaCO_3$ system.

As the concentration of PMPC is 15 g/L, the morphology of $BaCO_3$ crystals is very different, as shown in Figure 7. Uniform

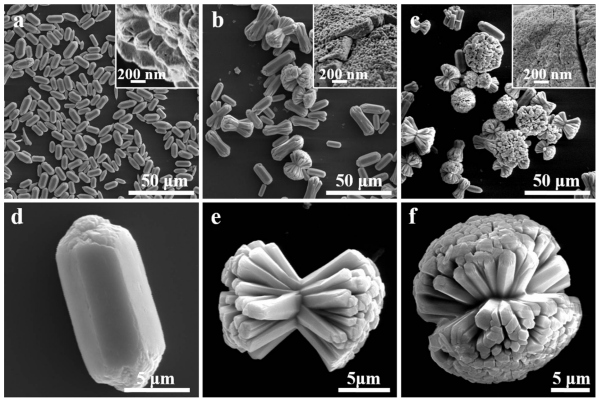

Figure 7. SEM images of $BaCO_3$ crystals prepared after different mineralization time in 15 g/L PMPC solution at 25 °C: (a, d) 3 h, (b, e) 6 h, and (c, f) 18 h.

rods with six symmetric sides are obtained in the early stage of mineralization. The enlarged image shows that the tips of them are rugged and composed of plenty of subunits (Figure 7a, d). As we know, $BaCO_3$ belongs to orthorhombic phase. Previous works have proved that the subunits of $BaCO_3$ crystals are needle-like, thus the rod-like crystals in present work probably are formed by the stacking of needle-like subunits under the

DOI: 10.1021/acssuschemeng.5b00387
ACS Sustainable Chem. Eng. 2015, 3, 1810−1818

control of PMPC.[30,39,49] Interestingly, both $CaCO_3$ and $BaCO_3$ crystals generated in 15 g/L PMPC solution have six sides or facets on their surfaces, and it may have some connection to and result from the strong regulation of PMPC during the growth process. The TEM and HRTEM images of $BaCO_3$ crystals are also obtained (Figure 8a, b), the clear and ordered

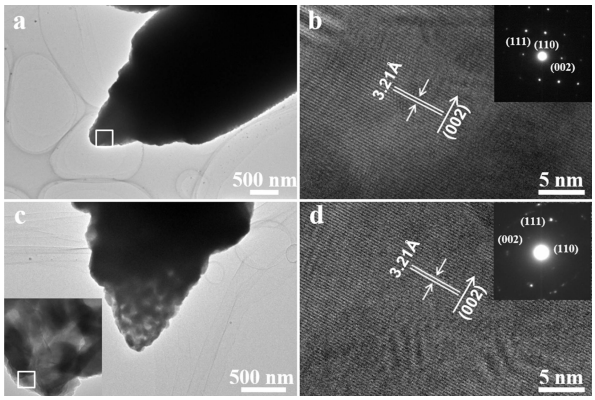

Figure 8. TEM images of $BaCO_3$ crystals prepared after 3 h mineralization time in 15 g/L PMPC solution at 25 °C: (a) undissolved $BaCO_3$ crystal; (b) HRTEM image of the marked area in (a), inset shows the SAED pattern; (c) partly dissolved $BaCO_3$ crystal, inset shows the enlarged image of (c); (d) HRTEM image of the marked area in (c), inset shows the SAED pattern.

lattice fringes indicate the particles are well crystallized, and the *d*-spacings of lattice fringes are 3.21 Å, corresponding to the (002) faces of witherite. Moreover, the sharp, single-crystalline SAED pattern with bright faculae also indicates that the crystals have a high crystallographic orientation.[50] The XRD patterns further confirm that the particles are well-crystallized witherite with the main peak at 24 ° ((111) face) (Figure S8, Supporting Information). When the mineralization time is increased to 6 h, the rod crystals reduce sharply, and instead, many bigger dumbbell-shaped crystals that are formed by the dendritic stacking of many rod-like subunits are generated (Figure 7b). Noticeably, these rod-like subunits also have six sides on the surface, which is similar to the morphology of particles obtained after 3 h reaction (Figure 7e). Moreover, the magnified SEM image also shows that these rod-like subunits are formed by the dense stacking of needle-like nanocrystals. Because of the appearance of bigger and reduction of rod crystals, it is not unreasonable that these dumbbell-shaped crystals are formed by consuming rods in an Ostwald repining process.[51]

Interestingly, we fortunately find that some rod crystals have been partly dissolved after only 3 h mineralization (Figure 8c). The magnified image shows the defect is very obvious and severe, which forcefully confirms our speculation. This destruction probably results from the fusion of regions whose crystal lattices are destroyed by PMPC chains and the release of PMPC chains. The TGA curves reveal that the concentration of residual PMPC in $BaCO_3$ is much more than that in initial solution; thus, PMPC chains are easy to release when $BaCO_3$ crystals are destroyed (Figure S9 and Table S1, Supporting Information). Although HRTEM image shows the lattice fringes are still clear and ordered with a *d*-spacings of 3.21 Å, the faculae on the SAED patterns are pale and fuzzy, indicating that the high crystallographic orientation is destroyed (Figure 8d). As the mineralization time is prolonged to 18 h, the dumbbell-shaped crystals further grow to twined spheres, which is similar to the results we have reported previously (Figure 7c, f).[49,50] It can be clearly found that these particles are also formed by the dendritic stacking of rod-like subunits with six symmetric sides on the surface. Expectedly, the rods crystals that are observed after 3 h reaction almost disappear. To further confirm our speculation, we also capture the structure of residual rod crystals after 18 h mineralization by TEM image. As shown in Figure S10 of the Supporting Information, the crystal is severely dissolved and some regions are hollowed-out. Besides, some needle-like subunits can be clearly observed in dissolved area, confirming that these crystals are formed by the aggregation of needle-like nanocrystals. This result further demonstrates that the dendritic crystals are formed by the consumption of rod crystals, which is in accord with Ostwald ripening theory.

Mechanism for Crystallization of $CaCO_3$ and $BaCO_3$ Crystals. A probable crystallization mechanism for the growth of $CaCO_3$ and $BaCO_3$ crystals was proposed based on the above results, as shown in Figure 9. Because the MPC monomer contains both positive and negative charges, the electrostatic interaction between different PMPC chains or different units on one chain is very strong. Compared with uncharged polymers that tend to become random coils in aqueous solution, the conformation of zwitterionic PMPC chains are partly restricted by charges that are located on side chains. Undoubtedly, like other polyelectrolytes, the metal ions (Ca^{2+} and Ba^{2+}) are favorable to aggregate around the charged regions by the strong cation-binding ability of the negative charge. Because of the high concentration of metal ions in this area, amorphous particles are first formed via the heteroge-

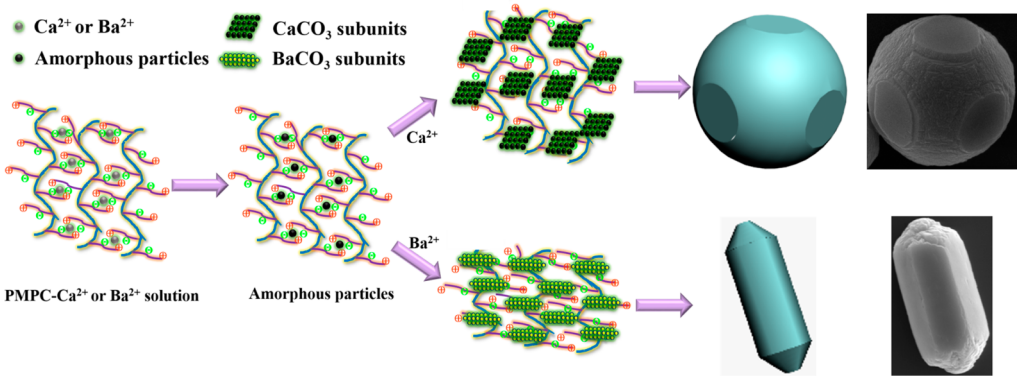

Figure 9. Schematic illustration of the $CaCO_3$ and $BaCO_3$ crystals' morphological evolution under the control of PMPC.

DOI: 10.1021/acssuschemeng.5b00387
ACS Sustainable Chem. Eng. 2015, 3, 1810−1818

neous nucleation.[5,52] The high density of charges would stabilize amorphous particles and prolong the lifetime of them, which has already been demonstrated by previous works.[10,39,53] Thus, we can capture the ACC in the early stage of $CaCO_3$ crystallization. With an increase in reaction time, the CO_3^{2-} in solution is evidently enhanced, resulting in more and more metal carbonates being formed along with the amorphous particles beginning to transform to the crystal phase.

At this moment, the interior unit-cell parameter of different metal carbonates would determine the morphology of subunits that would stack to form bigger crystals and further impact the final morphology of the crystals. For $CaCO_3$, the crystal cell belongs to the trigonal system, and it is likely to form rhombohedral subunits.[17] The final crystals should be composed of these rhombohedral subunits, which have been certified by the TEM and SEM images (Figure 5 and Figure S4, Supporting Information). Previous works have reported that $CaCO_3$ subunits tend to radially stack from the nucleation sites to form spherical particles due to the ion gradient around charged areas.[54] In the present work, the rhombohedral subunits would like to radially stack to form spheres under the control of the functional groups on PMPC because of the ion gradient around charged areas and the minimization of surface energy principle (Figure 6d).[9] During the stacking process, neighboring smaller subunits are partly fused and recrystallized to form dense and larger crystals with the intercalation of PMPC chains. With increasing mineralization time, the particles become bigger with six smooth and symmetrically distributed facets appearing. As we know, the equilibrium shape of calcite is a rhombohedron that has a six-sided structure. Thereby, the smooth facets are probably derived from a new mode of growth (crystal faceting) as the concentration of modifying PMPC in the solution is dropped. Moreover, previous reports have demonstrated these smooth facets are ascribed to the (104) faces of calcite, which is usually observed in the presence of a polymer modifier.[9,34] It is not unreasonable that the charged groups on the side chains of PMPC are the crucial factor for stabilizing spherical calcite with a six-sided structure.

For $BaCO_3$, the crystal cell belongs to the orthorhombic phase, resulting in the subunits likely to be needle-like.[10,55−57] In the early stage, the needle-like subunits tend to stack in parallel to form rod-like particles and part of PMPC chains, which have already been incorporated into or absorbed onto subunits that have been extruded. This is conforming to the nonclassical crystallization process first proposed by Colfen and Antonietti et al.,[17,58] that is, both the fusion of the crystalline units and the extrusion of polymers from aggregated crystals are involved in the crystallization process.[49,50] Interestingly, these rod-like particles have six symmetric sides, probably resulting from the stabilizing effect of PMPC on the facets of witherite. Due to the extrusion of PMPC chains in the early stage, the local PMPC concentration is higher around the tip of the rod-like crystal, which has already been demonstrated in our previous work by the simulation method.[49] Thus, the Ba^{2+} ions would like to aggregate on the tip of the rod-like crystal for the strong electrostatic interaction; undoubtedly, the tips are prior to growth compared with the middle part. Like other polymers or proteins, the volume occupancy and electrostatic interaction of these zwitterionic PMPC chains, which are intensified in the tips of the rod-like $BaCO_3$ crystals, will prevent the needle-like subunits from the further random and parallel stacking; instead, this urges the subunits to stack with a small angle between each other.[34,49] Following such a process, the dendritic $BaCO_3$ particles are formed with an increase in particle size.

CONCLUSION

In summary, uniform spherical $CaCO_3$ crystals and dumbbell-shaped $BaCO_3$ crystals were successfully prepared in the presence of PMPC as growth modifier via a gas−liquid diffusion reaction. The $CaCO_3$ particles had six smooth facets symmetrically distributed on the surface, and $BaCO_3$ particles were dendritically stacked by rod-like subunits that also had six sides on the surface. The results demonstrated that both the morphologies of $CaCO_3$ and $BaCO_3$ crystals could be effectively tuned by changing the crystallization time and the concentration of PMPC. The morphological evolution of $CaCO_3$ crystals under the control of PMPC was traced by time-resolved experiments, and both the ACC intermediate and dissolution−recrystallization processes of $CaCO_3$ particles were observed during the crystallization process. Because PMPC contains both positive and negative charges, which is similar to protein, we thought our work might provide a new view to the investigation of the mechanism of biomimetic mineralization under the control of protein. Moreover, the excellent water solubility, strong intermolecular association through charges, and high affinity for metal salts determined that PMPC might be a promising and versatile modifier for the morphology regulation of metal carbonate crystals.

ASSOCIATED CONTENT

Supporting Information

Description related to of TGA curves MPC and PMPC (Figure S1), FTIR spectra of PMPC and $CaCO_3$ prepared with PMPC (Figure S3), time-resolved SEM images (Figure S2 and S4) and Raman spectra (Figure S6) of $CaCO_3$ particles under the control of PMPC, EDS pattern of $CaCO_3$ particles (Figure S5), SEM images of $BaCO_3$ crystals prepared in different PMPC solutions (Figure S7), XRD patterns of $BaCO_3$ crystals generated with 15 g/L PMPC after different mineralization time (Figure S8), TGA curves of $BaCO_3$ crystals prepared in different PMPC solutions (Figure S9), and TEM image of $BaCO_3$ crystals generated with 15 g/L PMPC after 18 h reaction (Figure S10). The Supporting Information is available free of charge on the ACS Publications website at DOI: 10.1021/acssuschemeng.5b00387.

AUTHOR INFORMATION

Corresponding Author

* E-mail: peiyiwu@fudan.edu.cn. (P. Wu.).

Notes

The authors declare no competing financial interest.

ACKNOWLEDGMENTS

We gratefully thanks for the financial support of the National Science Foundation of China (NSFC) (20934002, 20774022) and the National Basic Research Program of China (2009CB930000).

REFERENCES

(1) Mann, S.; Heywood, B. R.; Rajam, S.; Birchall, J. D. Interfacial Control of Nuceation of Calcium-Carbonate under Organized Stearic-Acid Monolayers. *Proc. R. Soc. London, Ser. A* **1989**, *423*, 457−&.

(2) Picker, A.; Nuss, H.; Guenoun, P.; Chevallard, C. Polymer Vesicles as Microreactors for Bioinspired Calcium Carbonate Precipitation. *Langmuir* **2011**, *27*, 3213−3218.

DOI: 10.1021/acssuschemeng.5b00387
ACS Sustainable Chem. Eng. 2015, 3, 1810−1818

(3) Mann, S.; Ozin, G. A. Synthesis of Inorganic Materials with Complex Form. *Nature* **1996**, *382*, 313−318.
(4) Zhang, X.; Fan, Z.; Lu, Q.; Huang, Y.; Kaplan, D. L.; Zhu, H. Hierarchical Biomineralization of Calcium Carbonate Regulated by Silk Microspheres. *Acta Biomater.* **2013**, *9*, 6974−6980.
(5) Wang, X.; Bai, H.; Jia, Y.; Zhi, L.; Qu, L.; Xu, Y.; Li, C.; Shi, G. Synthesis of $CaCO_3$/graphene Composite Crystals for Ultra-Strong Structural Materials. *RSC Adv.* **2012**, *2*, 2154−2160.
(6) Choi, B. G.; Yang, M. H.; Park, T. J.; Huh, Y. S.; Lee, S. Y.; Hong, W. H.; Park, H. Programmable Peptide-Directed Two Dimensional Arrays of Various Nanoparticles on Graphene Sheets. *Nanoscale* **2011**, *3*, 3208−3213.
(7) Domingo, C.; Loste, E.; Gomez-Morales, J.; Garcia-Carmona, J.; Fraile, J. Calcite Precipitation by a High-Pressure CO_2 Carbonation Route. *J. Supercrit. Fluid.* **2006**, *36*, 202−215.
(8) Meldrum, F. C.; Coelfen, H. Controlling Mineral Morphologies and Structures in Biological and Synthetic Systems. *Chem. Rev.* **2008**, *108*, 4332−4432.
(9) Song, R. Q.; Xu, A. W.; Antonietti, M.; Colfen, H. Calcite Crystals with Platonic Shapes and Minimal Surfaces. *Angew. Chem., Int. Ed.* **2009**, *48*, 395−399.
(10) Yu, S. H.; Colfen, H. Bio-inspired Crystal Morphogenesis by Hydrophilic Polymers. *J. Mater. Chem.* **2004**, *14*, 2124−2147.
(11) Bots, P.; Benning, L. G.; Rodriguez-Blanco, J.-D.; Roncal-Herrero, T.; Shaw, S. Mechanistic Insights into the Crystallization of Amorphous Calcium Carbonate (ACC). *Cryst. Growth Des.* **2012**, *12*, 3806−3814.
(12) Ihli, J.; Kim, Y.-Y.; Noel, E. H.; Meldrum, F. C. The Effect of Additives on Amorphous Calcium Carbonate (ACC): Janus Behavior in Solution and the Solid State. *Adv. Funct. Mater.* **2013**, *23*, 1575−1585.
(13) Colfen, H.; Mann, S. Higher-order Organization by Mesoscale Self-assembly and Transformation of Hybrid Nanostructures. *Angew. Chem., Int. Ed.* **2003**, *42*, 2350−2365.
(14) Song, R. Q.; Colfen, H.; Xu, A. W.; Hartmann, J.; Antonietti, M. Polyelectrolyte-Directed Nanoparticle Aggregation: Systematic Morphogenesis of Calcium Carbonate by Nonclassical Crystallization. *ACS Nano* **2009**, *3*, 1966−1978.
(15) Liu, R.; Wu, D.; Liu, S.; Koynov, K.; Knoll, W.; Li, Q. An Aqueous Route to Multicolor Photoluminescent Carbon Dots Using Silica Spheres as Carriers. *Angew. Chem., Int. Ed.* **2009**, *48*, 4598−4601.
(16) Wang, X. Q.; Sun, H. L.; Xia, Y. Q.; Chen, C. X.; Xu, H.; Shan, H. H.; Lu, J. R. Lysozyme Mediated Calcium Carbonate Mineralization. *J. Colloid Interface Sci.* **2009**, *332*, 96−103.
(17) Wang, T. P.; Antonietti, M.; Colfen, H. Calcite Mesocrystals: "Morphing" Crystals by a Polyelectrolyte. *Chem.—Eur. J.* **2006**, *12*, 5722−5730.
(18) Cantaert, B.; Kim, Y.-Y.; Ludwig, H.; Nudelman, F.; Sommerdijk, N. A. J. M.; Meldrum, F. C. Think Positive: Phase Separation Enables a Positively Charged Additive to Induce Dramatic Changes in Calcium Carbonate Morphology. *Adv. Funct. Mater.* **2012**, *22*, 907−915.
(19) Li, H.; Xin, H. L.; Kunitake, M. E.; Keene, E. C.; Muller, D. A.; Estroff, L. A. Calcite Prisms from Mollusk Shells (*Atrina rigida*): Swiss-cheese-like Organic-Inorganic Single-crystal Composites. *Adv. Funct. Mater.* **2011**, *21*, 2028−2034.
(20) Xiao, J.; Yang, S. Polymorphic and Morphological Selection of $CaCO_3$ by Magnesium-Assisted Mineralization in Gelatin: Magnesium-Rich Spheres Consisting of Centrally Aligned Calcite Nanorods and Their Good Mechanical Properties. *CrystEngComm* **2011**, *13*, 2472−2478.
(21) Guo, X. H.; Liu, L.; Wang, W.; Zhang, J.; Wang, Y. Y.; Yu, S. H. Controlled Crystallization of Hierarchical and Porous Calcium Carbonate Crystals Using Polypeptide Type Block Copolymer as Crystal Growth Modifier in A Mixed Solution. *CrystEngComm* **2011**, *13*, 2054−2061.
(22) Yan, D. Y.; Yao, Y.; Dong, W. Y.; Zhu, S. M.; Yu, X. H. Novel Morphology of Calcium Carbonate Controlled by Poly(L-lysine). *Langmuir* **2009**, *25*, 13238−13243.
(23) Zhang, Z. P.; Gao, D. M.; Zhao, H.; Xie, C. G.; Guan, G. J.; Wang, D. P.; Yu, S. H. Biomimetic Assembly of Polypeptide-Stabilized $CaCO_3$ Nanoparticles. *J. Phys. Chem. B* **2006**, *110*, 8613−8618.
(24) Long, X.; Ma, Y.; Cho, K. R.; Li, D.; De Yoreo, J. J.; Qi, L. Oriented Calcite Micropillars and Prisms Formed through Aggregation and Recrystallization of Poly(Acrylic Acid) Stabilized Nanoparticles. *Cryst. Growth Des.* **2013**, *13*, 3856−3863.
(25) Sun, Z.-W.; An, Q.-F.; Zhao, Q.; Shangguan, Y.-G.; Zheng, Q. Study of Polyelectrolyte Complex Nanoparticles as Novel Templates for Biomimetic Mineralization. *Cryst. Growth Des.* **2012**, *12*, 2382−2388.
(26) Chu, H.; Liu, N.; Wang, X.; Jiao, Z.; Chen, Z. Morphology and In Vitro Release Kinetics of Drug-Loaded Micelles Based on Well-Defined PMPC-b-PBMA Copolymer. *Int. J. Pharm.* **2009**, *371*, 190−196.
(27) Wang, H. W.; Miyamoto, A.; Hirano, T.; Seno, M.; Sato, T. Radical Polymerization of 2-Methacryloyloxyethyl Phosphorylcholine in Water: Kinetics and Salt Effects. *Eur. Polym. J.* **2004**, *40*, 2287−2290.
(28) Ueda, T.; Oshida, H.; Kurita, K.; Ishihara, K.; Nakabayashi, N. Preparation of 2-Methacryloyloxyethyl Phosphorylcholine Copolymers with Alkyl Methacrylates and Their Blood Compatibility. *Polym. J.* **1992**, *24*, 1259−1269.
(29) Yusa, S. I.; Fukuda, K.; Yamamoto, T.; Ishihara, K.; Morishima, Y. Synthesis of Well-Defined Amphiphilic Block Copolymers Having Phospholipid Polymer Sequences as a Novel Blocompatible Polymer Micelle Reagent. *Biomacromolecules* **2005**, *6*, 663−670.
(30) Moro, T.; Takatori, Y.; Ishihara, K.; Konno, T.; Takigawa, Y.; Matsushita, T.; Chung, U.-i.; Nakamura, K.; Kawaguchi, H. Surface Grafting of Artificial Joints with a Biocompatible Polymer for Preventing Periprosthetic Osteolysis. *Nat. Mater.* **2004**, *3*, 829−836.
(31) Liu, G.; Jin, Q.; Liu, X.; Lv, L.; Chen, C.; Ji, J. Biocompatible Vesicles Based on PEO-b-PMPC/Alpha-Cyclodextrin Inclusion Complexes for Drug Delivery. *Soft Matter* **2011**, *7*, 662−669.
(32) Ma, I. Y.; Lobb, E. J.; Billingham, N. C.; Armes, S. P.; Lewis, A. L.; Lloyd, A. W.; Salvage, J. Synthesis of Biocompatible Polymers. 1. Homopolymerization of 2-Methacryloyloxyethyl Phosphorylcholine via ATRP in Protic Solvents: an Optimization Study. *Macromolecules* **2002**, *35*, 9306−9314.
(33) Ladj, R.; Bitar, A.; Eissa, M. M.; Fessi, H.; Mugnier, Y.; Le Dantec, R.; Elaissari, A. Polymer Encapsulation of Inorganic Nanoparticles for Biomedical Applications. *Int. J. Pharm.* **2013**, *458*, 230−241.
(34) Li, W.; Wu, P. Biomimetic Synthesis of Monodisperse Rosette-Like Calcite Mesocrystals Regulated by Carboxymethyl Cellulose and The Proposed Mechanism: an Unconventional Rhombohedra-Stacking Route. *CrystEngComm* **2009**, *11*, 2466−2474.
(35) Wang, J.; Li, X. Interpenetrating Polymer Network Hydrogels Based on Silicone and Poly(2-Methacryloyloxyethyl Phosphorylcholine). *Polym. Adv. Technol.* **2011**, *22*, 2091−2095.
(36) Xu, J. M.; Yuan, Y. L.; Shan, B.; Shen, J.; Lin, S. C. Ozone-Induced Grafting Phosphorylcholine Polymer onto Silicone Film Grafting 2-Methacryloyloxyethyl Phosphorylcholine onto Silicone Film to Improve Hemocompatibility. *Colloids Surf., B* **2003**, *30*, 215−223.
(37) Li, W.; Yu, Q. S.; Wu, P. Y. Submicronic Calcite Particles with Controlled Morphology Tailored by Polymer Skeletons via Carbonation Route with Compressed or Supercritical CO_2. *Green Chem.* **2009**, *11*, 1541−1549.
(38) Wehrmeister, U.; Soldati, A. L.; Jacob, D. E.; Haeger, T.; Hofmeister, W. Raman Spectroscopy of Synthetic, Geological and Biological Vaterite: a Raman Spectroscopic Study. *J. Raman Spectrosc.* **2010**, *41*, 193−201.
(39) Xu, S.; Wu, P. Monodisperse Spherical $CaCO_3$ Superstructure Self-Assembled by Vaterite Lamella under Control of Regenerated Silk Fibroin via Compressed CO_2. *CrystEngComm* **2013**, *15*, 5179−5188.
(40) Shen, Q.; Chen, Y. K.; Wei, H.; Zhao, Y.; Wang, D. J.; Xu, D. F. Suspension Effect of Poly(styrene-ran-methacrylic acid) Latex Particles

DOI: 10.1021/acssuschemeng.5b00387
ACS Sustainable Chem. Eng. 2015, 3, 1810−1818

on Crystal Growth of Calcium Carbonate. *Cryst. Growth Des.* **2005**, *5*, 1387−1391.
(41) Matsuda, Y.; Kobayashi, M.; Annaka, M.; Ishihara, K.; Takahara, A. Dimensions of a Free Linear Polymer and Polymer Immobilized on Silica Nanoparticles of a Zwitterionic Polymer in Aqueous Solutions with Various Ionic Strengths. *Langmuir* **2008**, *24*, 8772−8778.
(42) Shen, Q.; Wei, H.; Zhou, Y.; Huang, Y. P.; Yang, H. R.; Wang, D. J.; Xu, D. F. Properties of Amorphous Calcium Carbonate and The Template Action of Vaterite Spheres. *J. Phys. Chem. B* **2006**, *110*, 2994−3000.
(43) Raz, S.; Weiner, S.; Addadi, L. Formation of High-magnesian Calcites via an Amorphous Precursor Phase: Possible Biological Implications. *Adv. Mater.* **2000**, *12*, 38−42.
(44) Kim, Y.-Y.; Hetherington, N. B. J.; Noel, E. H.; Kroeger, R.; Charnock, J. M.; Christenson, H. K.; Meldrum, F. C. Capillarity Creates Single-Crystal Calcite Nanowires from Amorphous Calcium Carbonate. *Angew. Chem., Int. Ed.* **2011**, *50*, 12572−12577.
(45) Zhu, J.-H.; Yu, S.-H.; Xu, A.-W.; Coelfen, H. the Biomimetic Mineralization of Double-Stranded and Cylindrical Helical $BaCO_3$ Nanofibres. *Chem. Commun.* **2009**, *9*, 1106−1108.
(46) Colfen, H.; Antonietti, M. Mesocrystals: Inorganic Superstructures Made by Highly Parallel Crystallization and Controlled Alignment. *Angew. Chem., Int. Ed.* **2005**, *44*, 5576−5591.
(47) Geng, X.; Liu, L.; Jiang, J.; Yu, S.-H. Crystallization of $CaCO_3$ Mesocrystals and Complex Aggregates in a Mixed Solvent Media Using Polystyrene Sulfonate as a Crystal Growth Modifier. *Cryst. Growth Des.* **2010**, *10*, 3448−3453.
(48) Shen, D.; Li, W.; Xu, S.; Wu, P. Fabrication of $BaCO_3$ Sheaves Tailored by Carboxymethyl Cellulose under Compressed CO_2. *J. Cryst. Growth* **2012**, *353*, 101−107.
(49) Li, W.; Sun, S.; Yu, Q.; Wu, P. Controlling the Morphology of $BaCO_3$ Aggregates by Carboxymethyl Cellulose through Polymer Induced Needle-Stacking Self-Assembly. *Cryst. Growth Des.* **2010**, *10*, 2685−2692.
(50) Xu, S.; Wu, P. A Rapid, Green and Versatile Route to Synthesize Metal Carbonate Superstructures via the Combination of Regenerated Silk Fibroin and Compressed CO_2. *CrystEngComm* **2014**, *16*, 1311−1321.
(51) Lu, G.; Li, C.; Shi, G. Synthesis and Characterization of 3D Dendritic Gold Nanostructures and Their Use as Substrates for Surface-Enhanced Raman Scattering. *Chem. Mater.* **2007**, *19*, 3433−3440.
(52) Tjipto, E.; Quinn, J. F.; Caruso, F. Assembly of Multilayer Films from Polyelectrolytes Containing Weak and Strong Acid Moieties. *Langmuir* **2005**, *21*, 8785−8792.
(53) Ohgo, K.; Bagusat, F.; Asakura, T.; Scheler, U. Investigation of Structural Transition of Regenerated Silk Fibroin Aqueous Solution by Rheo-NMR Spectroscopy. *J. Am. Chem. Soc.* **2008**, *130*, 4182−4186.
(54) Grassmann, O.; Lobmann, P. Biomimetic Nucleation and Growth of $CaCO_3$ in Hydrogels Incorporating Carboxylate Groups. *Biomaterials* **2004**, *25*, 277−282.
(55) Yu, S. H.; Colfen, H.; Antonietti, M. Polymer-Controlled Morphosynthesis and Mineralization of Metal Carbonate Superstructures. *J. Phys. Chem. B* **2003**, *107*, 7396−7405.
(56) Yu, S. H.; Colfen, H.; Xu, A. W.; Dong, W. F. Complex Spherical $BaCO_3$ Superstructures Self-Assembled by a Facile Mineralization Process under Control of Simple Polyelectrolytes. *Cryst. Growth Des.* **2004**, *4*, 33−37.
(57) Ni, Y.; Zhang, H.; Hong, J.; Zhang, L.; Wei, X. PAM-Directed Fabrication, Shape Evolution and Formation Mechanism of $BaCO_3$ Crystals with Higher-Order Superstructures. *J. Cryst. Growth* **2008**, *310*, 4460−4467.
(58) Kulak, A. N.; Iddon, P.; Li, Y.; Armes, S. P.; Colfen, H.; Paris, O.; Wilson, R. M.; Meldrum, F. C. Continuous structural evolution of calcium carbonate particles: A unifying model of copolymer-mediated crystallization. *J. Am. Chem. Soc.* **2007**, *129* (12), 3729−3736.

DOI: 10.1021/acssuschemeng.5b00387
ACS Sustainable Chem. Eng. 2015, 3, 1810−1818